Supporting Information

Bischofs et al. 10.1073/pnas.0810878106

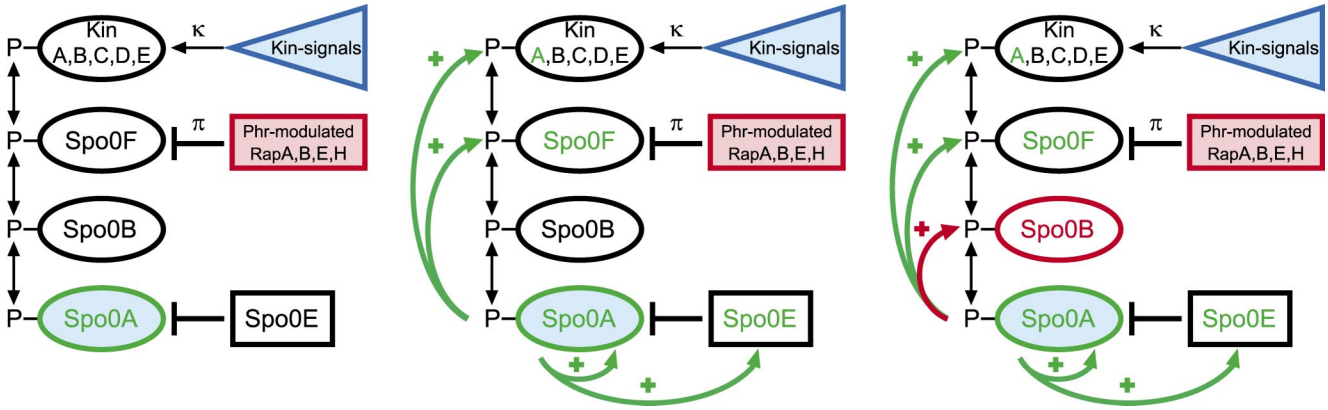

Fig. S1. Overview of schematic models considered for analyzing the role of ''low'' Spo0A~P-driven transcriptional feedback on signal integration. From left to right: Open loop system without feedback, closed loop ''wt''-model with ''low'' Spo0A~P feedback, and P_{spo0B}- loop ''mutant'' with an additional positive feedback upregulating Spo0B production.

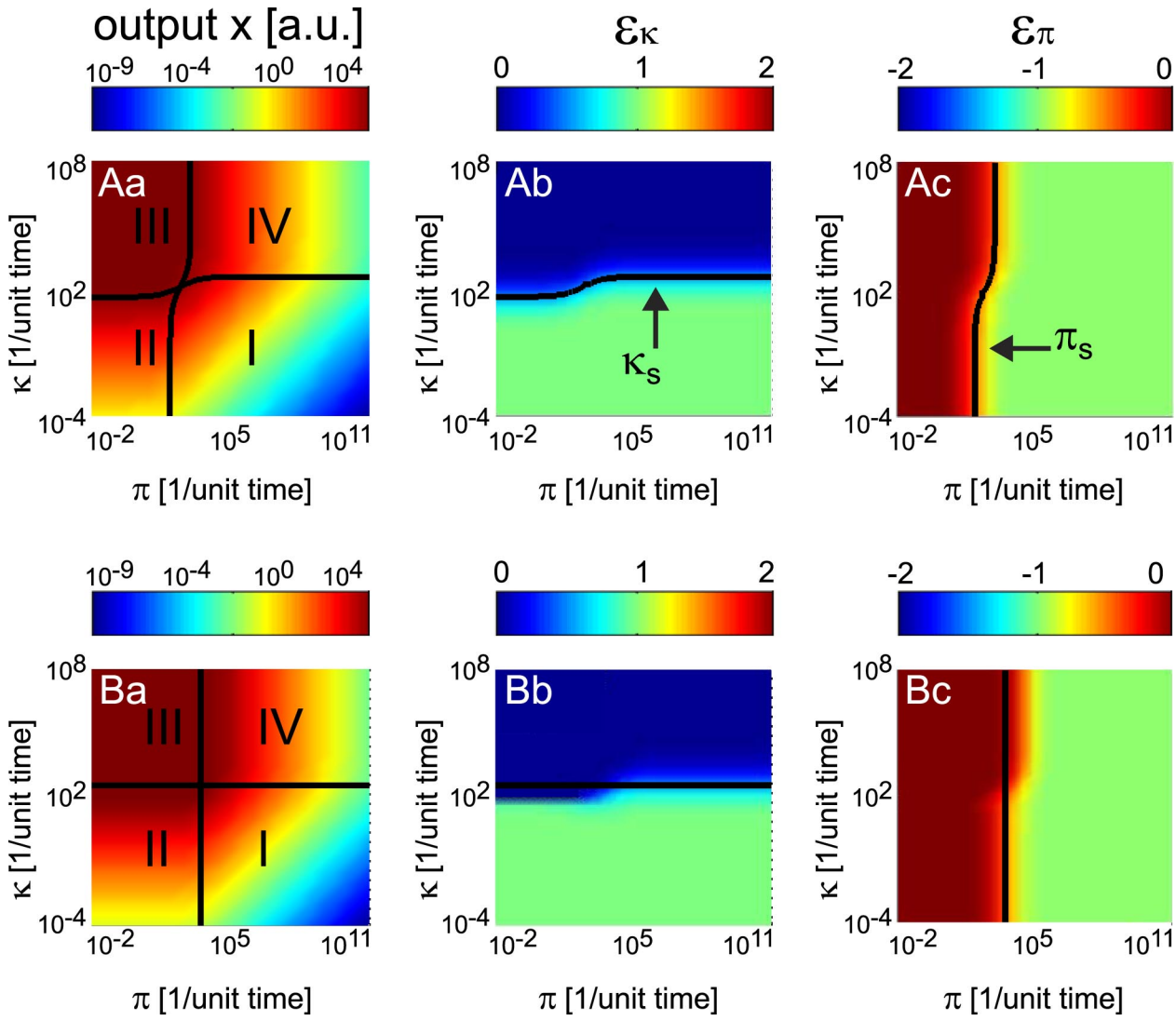

Fig. S2. Global output behavior and input sensitivities of a closed-loop system. (*A*) Results of a phosphorelay with equal forward and backward phosphoryl-transfer rates (top row). (*B*) A model with unequal rates with $k_i^f = 10k_i^b$ (bottom row). Within each row we show in *a* the global behavior of the input–output relation $f(\kappa,\pi)$ on a log–log scale. The control functions $\kappa_s(\pi)$ and $\pi_s(\kappa)$ partition the input space into 4 operating regimes I–IV. The signal regime I is located in the bottom right quadrant where the output describes diagonal iso-color lines characteristic for a ratiometric input coupling. In *b* we show the elasticity coefficient ε_κ and the analytic prediction for $\kappa_s(\pi)$ as a black line. In *c* we show the corresponding ε_π and $\pi_s(\kappa)$ as a black line. Deviating from the equal transfer-rate model does not result in any qualitative changes but generally alter $\tilde{\kappa}_s$ and $\tilde{\pi}_s$ that deviate from the equal-rate functions shown.

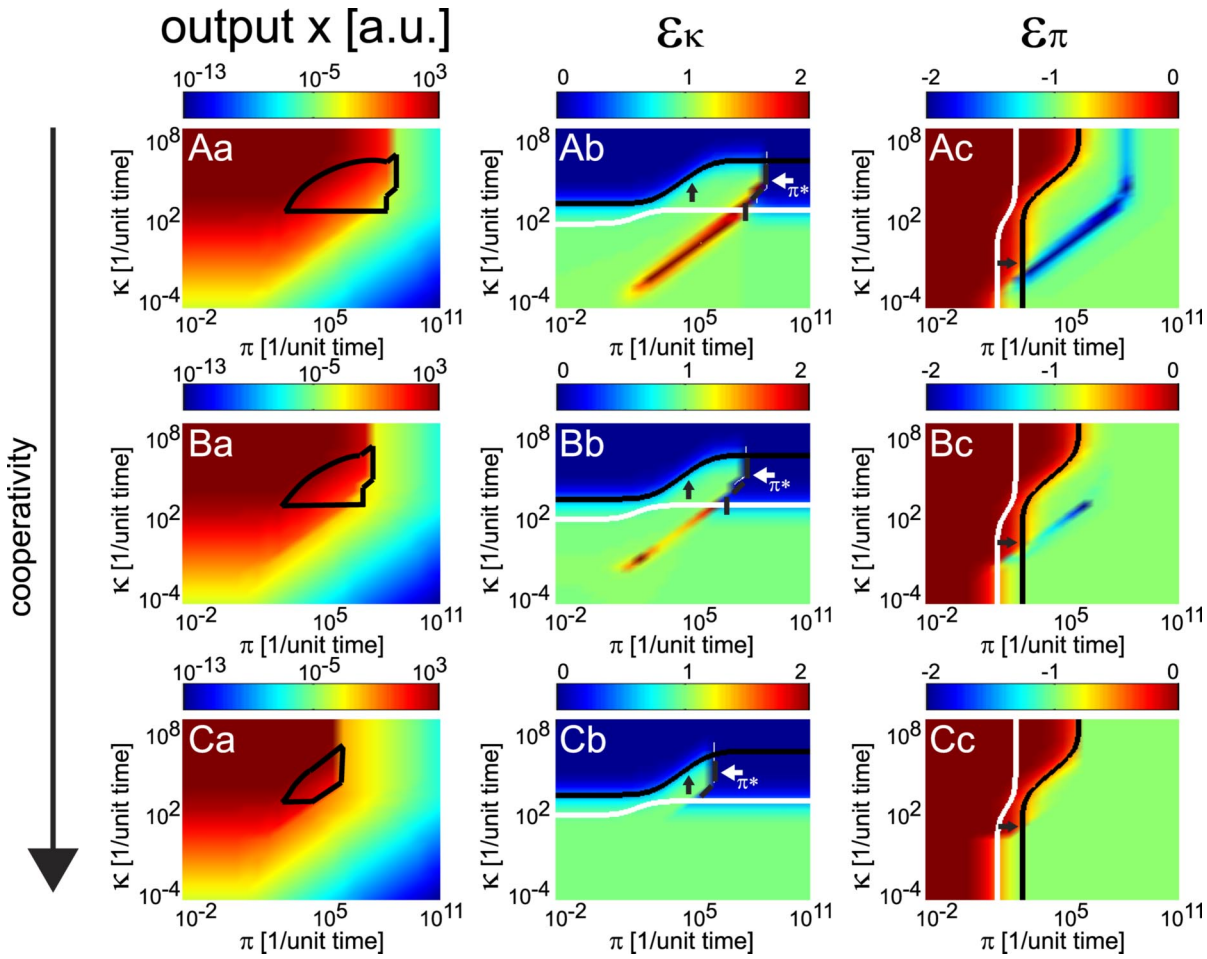

Fig. S3. Effect of different feedback mechanisms on expanding the signal-integration regime I with respect to the equivalent closed-loop model of Fig. S2. The rows show results for 3 different feedback models with identical K_i but different levels of cooperativity, namely a noncooperative feedback $n = 1$ (*A*), a cooperative Hill feedback with $n = 2$ (*B*), and an ideal switch-like feedback, $n = \infty$ (*C*). In each row we show in *a* the global behavior of the output. In all cases, feedback results in an increase in the regime I compared with the open-loop case. The black line outlines the gain in regime I with respect to the open-loop system and in this case spans several orders of magnitude. In *b* we show the elasticity coefficient ε_κ. Feedback shifts κ_s (black) to larger kinase inputs compared with the open-loop system (white). The arrow denotes π_{*h} where feedback is being turned off, and ε_κ falls back to the open-loop behavior. The diagonal stretch of increased $\varepsilon_\kappa > 1$ (red) in regime I is typical for a system with feedback operating in the nonlinear portion of its transfer function. In *c* we show the elasticity coefficient ε_π. Here, feedback has also resulted in an increase of π_s (black) compared with the open-loop system (white). Note the diagonal stretch of increased sensitivity $\varepsilon_\pi < -1$ that mirrors the behavior in ε_κ in regime I. The ratio of (κ/π) is still the relevant control parameter, but it increases the output in a nonlinear fashion. The corresponding unequal transfer-rate model resulted qualitatively in the same results (not shown).

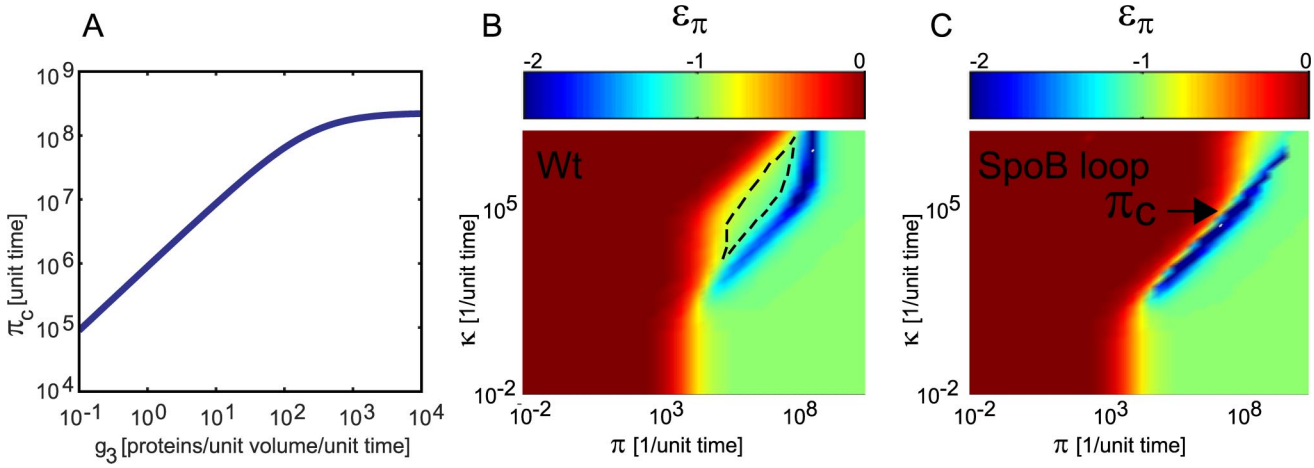

Fig. S4. Effect of Spo0B feedback on system behavior. (*A*) π_c increases monotonically as a function of the feedback gain g_3 onto Spo0B. (*B*) ε_π of the WT architecture. The feedback-enabled gain in regime I is circled. (*C*) ε_π for the same system as in *B* but with a Spo0B feedback of comparable strength with the other feedbacks. The Spo0B loop shifts π_c to larger phosphatase values and thus, diminishes the positive effect of the WT feedback onto the expansion of regime I. These plots were generated for the parameters given in the main text.

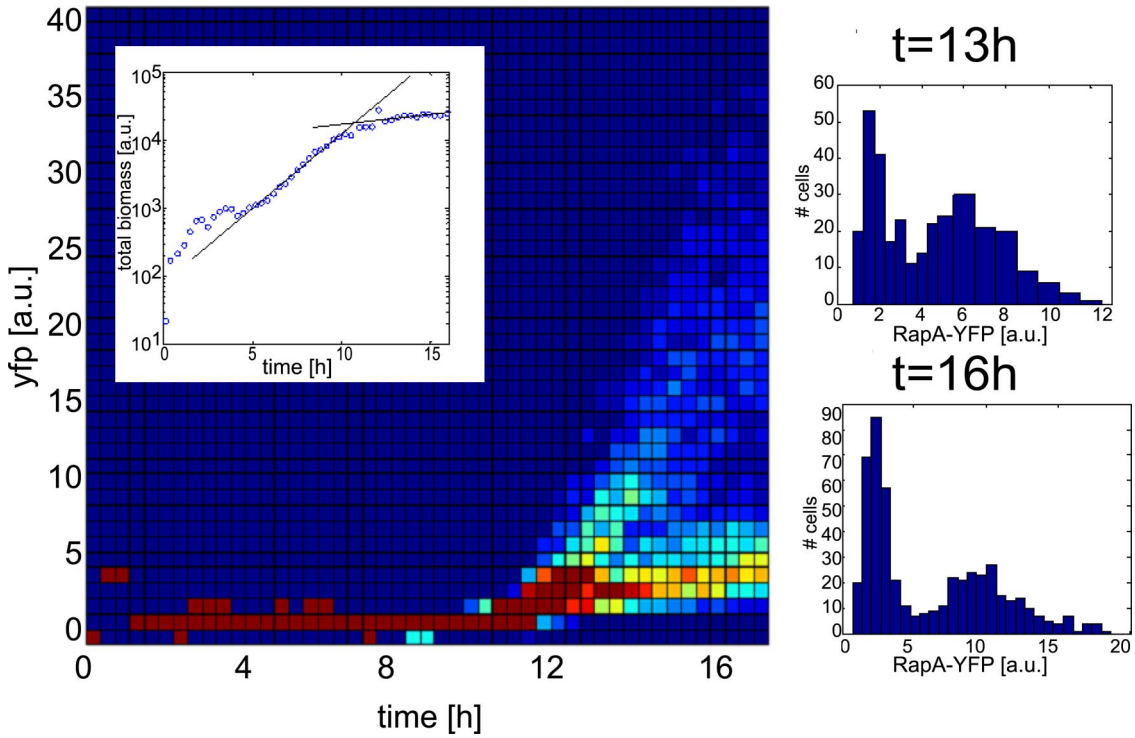

Fig. S5. RapA Bifurcation dynamics in a developing mircocolony: YFP dynamics emerging from P_{rapA}-*iyfp* within a micro-colony taken from a different experiment than the one shown in the article. *Inset* shows the recorded growth curve as estimated from the colony area obtained from image processing. A (rarely seen) single cell lysis event occurred at $t \approx 4$ h. The heat map shows the population frequency evolution of the fluorescence intensity in the microcolony (see description of Fig. 4 for more details). The histograms on the right show the fluorescence distribution at selected time points. The general features of the fluorescence and growth dynamics are robust, whereas certain aspects, such as the exact timing to reach T_0 and the relative proportions of the population splitting, vary from experiment to experiment.

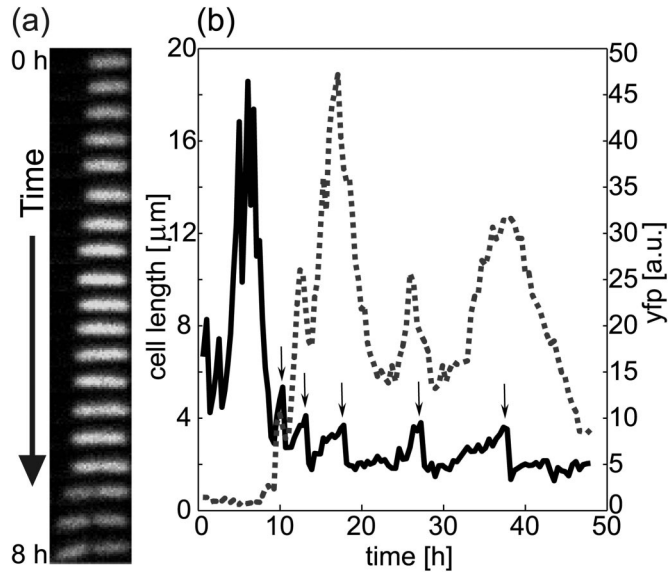

Fig. S6. Correlation of YFP production driven from the RapA operon and cell growth. (*a*) Snapshots of a growing cell in stationary phase. During period of cell growth P_{rapA}-*iyfp*-driven YFP intensity increases and then drops at cell division. (*b*) Cell length (solid) and YFP intensity (broken line) evolution for a representative cell trajectory. Arrows denote times of cell division. YFP production correlates nicely with periods of cell growth. Each cell division event is accompanied by a peak in P_{rapA}-driven fluorescence intensity.

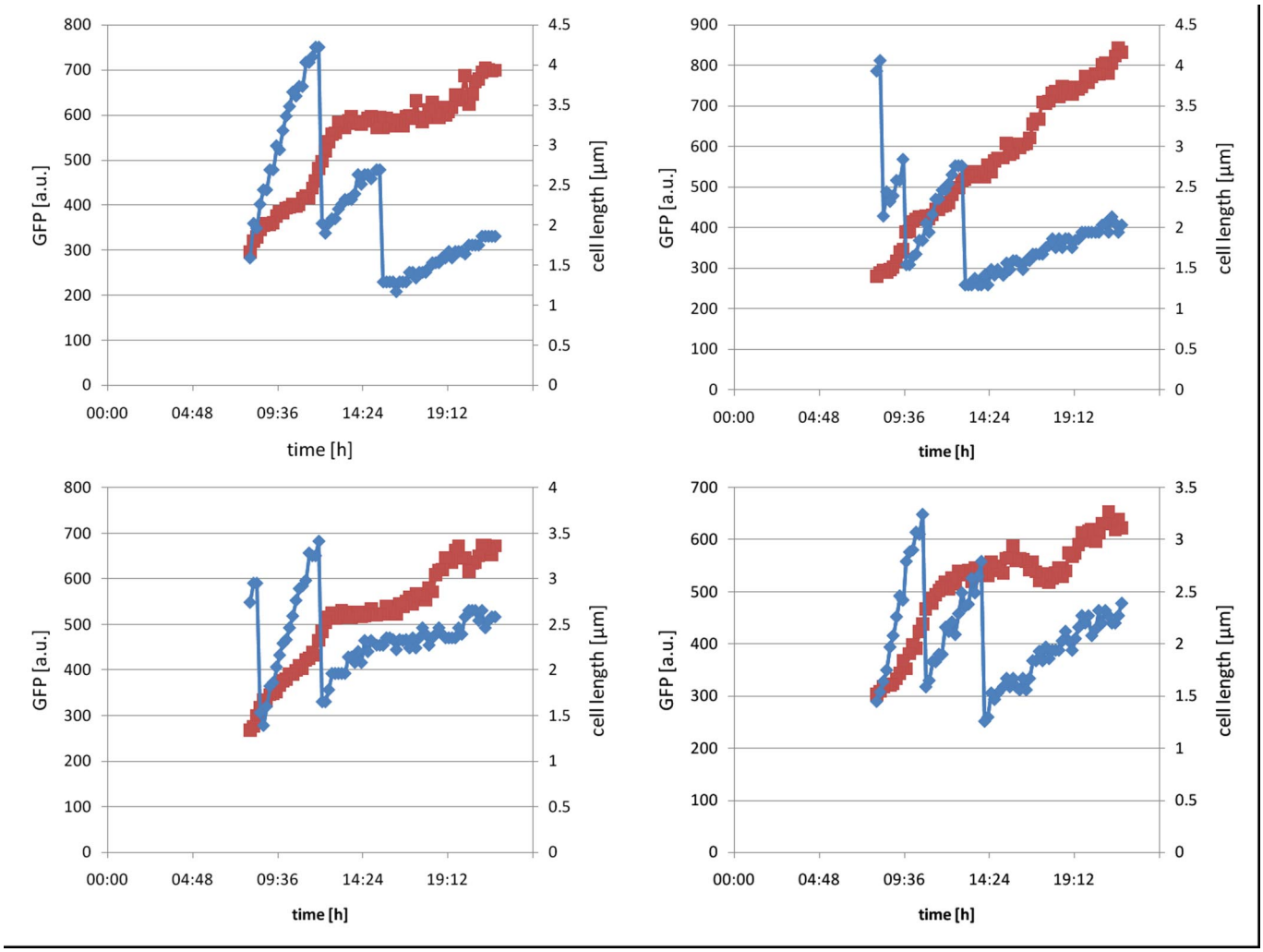

Fig. S7. Cell growth and GFP production from a constitutive nonnative promoter Ppenn. Four representative fluorescence (red) and length profile (blue) trajectories driven from amyE::P_{penn}-gfp integrated into B168 driving GFP from a constitutively active promoter (see Movie S2). The strain amyE::P_{penn}-gfp was a kind gift from Gavin Price (University of California, Berkeley, CA). It drives GFP from a nonnative Ppenn promoter that is constitutively on during vegetative growth in *Bacillus subtilis*. We show only a portion of the total fluorescence trajectory during the growth period where P_{rapA}-driven fluorescence shows a pulsatile behavior that is strongly correlated with cell cycle.

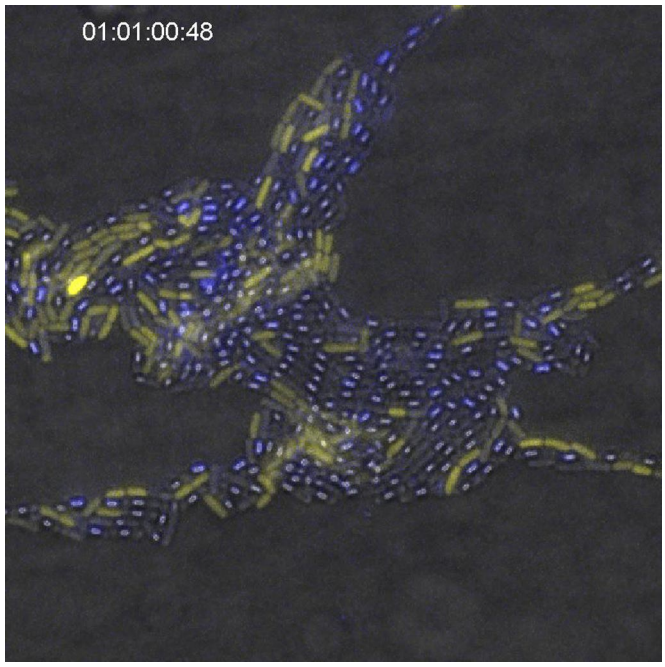

Movie S1. Development of a sporulating microcolony of strain rap/IIA (B168, P_{rapA}-*iyfp*, Cm^r, amyE::P_{spoIIA}-*icfp*, Km^r) on a nutrient-poor agar gel pad after growth in liquid growth medium. Bright-field images (gray) were digitally overlaid with fluorescence driven from P_{rapA} (yellow) and P_{spoIIA} (blue). Note that blue fluorescence within matured spores results from autofluorescence.

Movie S1 (AVI)

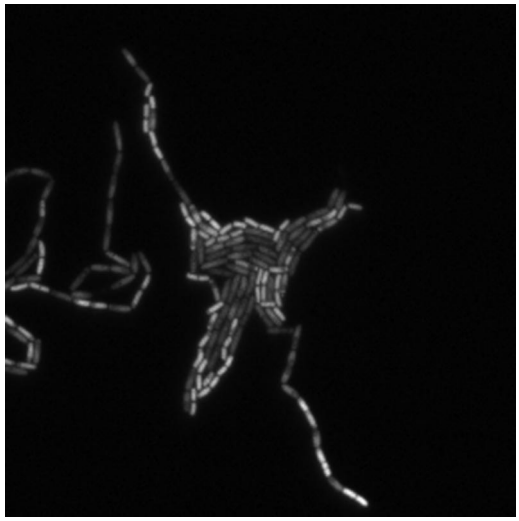

Movie S2. Development of a sporulating microcolony of strain P_{penn}-*gfp* (B168, amyE::P_{penn}-*gfp*, Cm^r). Bright-field (red) is overlaid with gfp fluorescence (green). The continued trend of rising in fluorescence is likely attributable to the constant strong expression of stable GFP in a slowly replicating cell that dominates the time scale to reach steady state via dilution of the fluorophore. Note that cells entering the sporulation pathway show decay in fluorescence over time, preferentially in the developing endospore. This may be due to differential σ-factor availability and/or unspecific protease activity.

Movie S2 (MPG)

Other Supporting Information Files

SI Appendix (PDF)